



Universiteit
Leiden

The Netherlands

Coherent electron focusing

Beenakker, C.W.J.; Houten, H. van; Wees, B.J. van

Citation

Beenakker, C. W. J., Houten, H. van, & Wees, B. J. van. (1989).
Coherent electron focusing. Retrieved from
<https://hdl.handle.net/1887/3336>

Version: Not Applicable (or Unknown)

License: [Leiden University Non-exclusive license](#)

Downloaded from: <https://hdl.handle.net/1887/3336>

Note: To cite this publication please use the final published version (if applicable).

Reprint

**FESTKÖRPER
PROBLEME
ADVANCES IN
SOLID STATE
PHYSICS**

Contents

1. <i>Introduction</i> (SILVERMIL 249)	1
2. <i>Background</i> (SILVERMIL 249)	2
3. <i>Objectives</i> (SILVERMIL 249)	3
4. <i>Organization</i> (SILVERMIL 249)	4
5. <i>Personnel</i> (SILVERMIL 249)	5
6. <i>Methods</i> (SILVERMIL 249)	6
7. <i>Results</i> (SILVERMIL 249)	7
8. <i>Conclusions</i> (SILVERMIL 249)	8
9. <i>Recommendations</i> (SILVERMIL 249)	9
10. <i>References</i> (SILVERMIL 249)	10
11. <i>Appendix</i> (SILVERMIL 249)	11
12. <i>Index</i> (SILVERMIL 249)	12
13. <i>Summary</i> (SILVERMIL 249)	13
14. <i>Notes</i> (SILVERMIL 249)	14
15. <i>Footnotes</i> (SILVERMIL 249)	15
16. <i>References</i> (SILVERMIL 249)	16
17. <i>Appendix</i> (SILVERMIL 249)	17
18. <i>Index</i> (SILVERMIL 249)	18
19. <i>Summary</i> (SILVERMIL 249)	19
20. <i>Notes</i> (SILVERMIL 249)	20
21. <i>Footnotes</i> (SILVERMIL 249)	21
22. <i>References</i> (SILVERMIL 249)	22
23. <i>Appendix</i> (SILVERMIL 249)	23
24. <i>Index</i> (SILVERMIL 249)	24
25. <i>Summary</i> (SILVERMIL 249)	25
26. <i>Notes</i> (SILVERMIL 249)	26
27. <i>Footnotes</i> (SILVERMIL 249)	27
28. <i>References</i> (SILVERMIL 249)	28
29. <i>Appendix</i> (SILVERMIL 249)	29
30. <i>Index</i> (SILVERMIL 249)	30
31. <i>Summary</i> (SILVERMIL 249)	31
32. <i>Notes</i> (SILVERMIL 249)	32
33. <i>Footnotes</i> (SILVERMIL 249)	33
34. <i>References</i> (SILVERMIL 249)	34
35. <i>Appendix</i> (SILVERMIL 249)	35
36. <i>Index</i> (SILVERMIL 249)	36
37. <i>Summary</i> (SILVERMIL 249)	37
38. <i>Notes</i> (SILVERMIL 249)	38
39. <i>Footnotes</i> (SILVERMIL 249)	39
40. <i>References</i> (SILVERMIL 249)	40
41. <i>Appendix</i> (SILVERMIL 249)	41
42. <i>Index</i> (SILVERMIL 249)	42
43. <i>Summary</i> (SILVERMIL 249)	43
44. <i>Notes</i> (SILVERMIL 249)	44
45. <i>Footnotes</i> (SILVERMIL 249)	45
46. <i>References</i> (SILVERMIL 249)	46
47. <i>Appendix</i> (SILVERMIL 249)	47
48. <i>Index</i> (SILVERMIL 249)	48
49. <i>Summary</i> (SILVERMIL 249)	49
50. <i>Notes</i> (SILVERMIL 249)	50
51. <i>Footnotes</i> (SILVERMIL 249)	51
52. <i>References</i> (SILVERMIL 249)	52
53. <i>Appendix</i> (SILVERMIL 249)	53
54. <i>Index</i> (SILVERMIL 249)	54
55. <i>Summary</i> (SILVERMIL 249)	55
56. <i>Notes</i> (SILVERMIL 249)	56
57. <i>Footnotes</i> (SILVERMIL 249)	57
58. <i>References</i> (SILVERMIL 249)	58
59. <i>Appendix</i> (SILVERMIL 249)	59
60. <i>Index</i> (SILVERMIL 249)	60
61. <i>Summary</i> (SILVERMIL 249)	61
62. <i>Notes</i> (SILVERMIL 249)	62
63. <i>Footnotes</i> (SILVERMIL 249)	63
64. <i>References</i> (SILVERMIL 249)	64
65. <i>Appendix</i> (SILVERMIL 249)	65
66. <i>Index</i> (SILVERMIL 249)	66
67. <i>Summary</i> (SILVERMIL 249)	67
68. <i>Notes</i> (SILVERMIL 249)	68
69. <i>Footnotes</i> (SILVERMIL 249)	69
70. <i>References</i> (SILVERMIL 249)	70
71. <i>Appendix</i> (SILVERMIL 249)	71
72. <i>Index</i> (SILVERMIL 249)	72
73. <i>Summary</i> (SILVERMIL 249)	73
74. <i>Notes</i> (SILVERMIL 249)	74
75. <i>Footnotes</i> (SILVERMIL 249)	75
76. <i>References</i> (SILVERMIL 249)	76
77. <i>Appendix</i> (SILVERMIL 249)	77
78. <i>Index</i> (SILVERMIL 249)	78
79. <i>Summary</i> (SILVERMIL 249)	79
80. <i>Notes</i> (SILVERMIL 249)	80
81. <i>Footnotes</i> (SILVERMIL 249)	81
82. <i>References</i> (SILVERMIL 249)	82
83. <i>Appendix</i> (SILVERMIL 249)	83
84. <i>Index</i> (SILVERMIL 249)	84
85. <i>Summary</i> (SILVERMIL 249)	85
86. <i>Notes</i> (SILVERMIL 249)	86
87. <i>Footnotes</i> (SILVERMIL 249)	87
88. <i>References</i> (SILVERMIL 249)	88
89. <i>Appendix</i> (SILVERMIL 249)	89
90. <i>Index</i> (SILVERMIL 249)	90
91. <i>Summary</i> (SILVERMIL 249)	91
92. <i>Notes</i> (SILVERMIL 249)	92
93. <i>Footnotes</i> (SILVERMIL 249)	93
94. <i>References</i> (SILVERMIL 249)	94
95. <i>Appendix</i> (SILVERMIL 249)	95
96. <i>Index</i> (SILVERMIL 249)	96
97. <i>Summary</i> (SILVERMIL 249)	97
98. <i>Notes</i> (SILVERMIL 249)	98
99. <i>Footnotes</i> (SILVERMIL 249)	99
100. <i>References</i> (SILVERMIL 249)	100
101. <i>Appendix</i> (SILVERMIL 249)	101
102. <i>Index</i> (SILVERMIL 249)	102
103. <i>Summary</i> (SILVERMIL 249)	103
104. <i>Notes</i> (SILVERMIL 249)	104
105. <i>Footnotes</i> (SILVERMIL 249)	105
106. <i>References</i> (SILVERMIL 249)	106
107. <i>Appendix</i> (SILVERMIL 249)	107
108. <i>Index</i> (SILVERMIL 249)	108
109. <i>Summary</i> (SILVERMIL 249)	109
110. <i>Notes</i> (SILVERMIL 249)	110
111. <i>Footnotes</i> (SILVERMIL 249)	111
112. <i>References</i> (SILVERMIL 249)	112
113. <i>Appendix</i> (SILVERMIL 249)	113
114. <i>Index</i> (SILVERMIL 249)	114
115. <i>Summary</i> (SILVERMIL 249)	115
116. <i>Notes</i> (SILVERMIL 249)	116
117. <i>Footnotes</i> (SILVERMIL 249)	117
118. <i>References</i> (SILVERMIL 249)	118
119. <i>Appendix</i> (SILVERMIL 249)	119
120. <i>Index</i> (SILVERMIL 249)	120
121. <i>Summary</i> (SILVERMIL 249)	121
122. <i>Notes</i> (SILVERMIL 249)	122
123. <i>Footnotes</i> (SILVERMIL 249)	123
124. <i>References</i> (SILVERMIL 249)	124
125. <i>Appendix</i> (SILVERMIL 249)	125
126. <i>Index</i> (SILVERMIL 249)	126
127. <i>Summary</i> (SILVERMIL 249)	127
128. <i>Notes</i> (SILVERMIL 249)	128
129. <i>Footnotes</i> (SILVERMIL 249)	129
130. <i>References</i> (SILVERMIL 249)	130
131. <i>Appendix</i> (SILVERMIL 249)	131
132. <i>Index</i> (SILVERMIL 249)	132
133. <i>Summary</i> (SILVERMIL 249)	133
134. <i>Notes</i> (SILVERMIL 249)	134
135. <i>Footnotes</i> (SILVERMIL 249)	135
136. <i>References</i> (SILVERMIL 249)	136
137. <i>Appendix</i> (SILVERMIL 249)	137
138. <i>Index</i> (SILVERMIL 249)	138
139. <i>Summary</i> (SILVERMIL 249)	139
140. <i>Notes</i> (SILVERMIL 249)	140
141. <i>Footnotes</i> (SILVERMIL 249)	141
142. <i>References</i> (SILVERMIL 249)	142
143. <i>Appendix</i> (SILVERMIL 249)	143
144. <i>Index</i> (SILVERMIL 249)	144
145. <i>Summary</i> (SILVERMIL 249)	145
146. <i>Notes</i> (SILVERMIL 249)	146
147. <i>Footnotes</i> (SILVERMIL 249)	147
148. <i>References</i> (SILVERMIL 249)	148
149. <i>Appendix</i> (SILVERMIL 249)	149
150. <i>Index</i> (SILVERMIL 249)	150

Coherent electron focusing

C. W. J. Beenakker

Philips Research Laboratories, 5600 JA Eindhoven, The Netherlands

H. van Houten

Philips Laboratories, Briarcliff Manor, NY 10510, USA

B. J. van Wees

Applied Physics, Delft University of Technology, 2600 GA Delft, The Netherlands

Summary: Theory and experiment are reviewed of the classical and quantum mechanical focusing by a magnetic field of ballistic electrons injected through a point contact in a two-dimensional electron gas. Two alternative points of view are emphasized. On the one hand, the experiment is a realization of electron optics in the solid state. The three basic building blocks are a coherent and monochromatic point source/detector, an electrostatic mirror with little diffuse scattering, and a magnetic lens. On the other hand, coherent electron focusing is a resistance measurement in the quantum ballistic transport regime, which exhibits the characteristic features of this regime in a most extreme way. For example, large magnetoresistance oscillations occur (up to 95% amplitude modulation is observed), with a periodicity which is non-locally determined by the separation between current and voltage point contacts. A WKB calculation of the transmission probabilities shows that this effect is the result of the interference of coherently excited magnetic edge states at the electron gas boundary. Another example is the absence of local equilibrium: The measurements show that the point contacts can selectively populate (and detect) specific Landau levels, and that this highly non-equilibrium population is maintained over distances of microns.

1 Introduction

Electron focusing in metals was pioneered by Sharvin [1] and Tsoi [2] as a powerful tool to investigate the shape of the Fermi surface, surface scattering, and the electron-phonon interaction [3]. The experiment is the analogue in the solid state of magnetic focusing in vacuum (e.g. in a β -spectrometer). Required is a large mean free path for the carriers at the Fermi surface, to ensure *ballistic* motion as in vacuum. The mean free path (which can be as large as 1 cm in pure metallic single crystals) should be much larger than the length L on which the focusing takes place. Experimentally $L = 10^{-2} - 10^{-1}$ cm is the separation of two metallic needles (point contacts) pressed on the crystal surface, which serve to inject a divergent electron beam and detect its focusing by the mag-

netic field. In metals, electron focusing is essentially a *classical* phenomenon because of the small Fermi wave length λ_F (typically 0.5 nm, on the order of the inter-atomic separation).

The Fermi wave length is 100 times as large in the two-dimensional electron gas (2DEG) which is present at the interface of a GaAs-AlGaAs heterostructure. This length scale is within reach of electron-beam lithography, while remaining well below the mean free path in high-mobility material ($10 \mu\text{m}$ can be realized at low temperatures in heterostructures grown by molecular-beam epitaxy). For these two reasons the *quantum ballistic* transport regime has become accessible in a 2DEG [4]. In the present paper theory and experiment are reviewed of electron focusing in this regime [5 – 8], which turns out to be strikingly different from the classical regime familiar from metals. This has motivated the new name: *coherent electron focusing*.

The geometry of the experiment (Fig. 1) is the transverse focusing geometry of Tsoi [2], and consists of two point contacts on the same boundary in a perpendicular magnetic field B . [In metals one can also use the geometry of Sharvin [1], with opposite point contacts in a longitudinal field. This is not possible in two dimensions.] Because the electron gas is confined to the interior of the heterostructure, one can not just use a metal needle to fabricate a point contact to a 2DEG. Instead, the point contacts are created electrostatically by depositing an electrode of a suitable shape on top of the heterostructure [9]. On applying a negative voltage to the split-gate electrode shown in Fig. 1 the electron gas underneath the gate structure is depleted, creating two 2DEG regions (i and c) electrically isolated from the rest of the 2DEG – apart from the two narrow and short constrictions (point contacts)

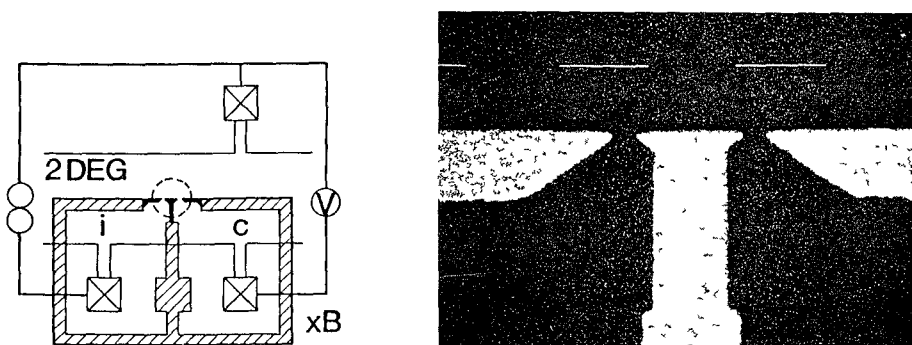


Fig. 1 Schematic layout (left) of the double point contact device for the electron focusing experiments (in a three-terminal measurement configuration). The crossed squares are ohmic contacts to the 2DEG. The split-gate (shaded) separates injector (i) and collector (c) areas from the bulk 2DEG. The fine details of the gate structure inside the dashed circle are shown in a scanning electron micrograph (right). The bar denotes a length of $1 \mu\text{m}$. In this device the point contact separation is $L = 1.5 \mu\text{m}$. A device with $L = 3.0 \mu\text{m}$ was also studied. [From Ref 8.]

under the 250 nm wide openings in the split-gate. The devices studied had point contact separations L of 1.5 and 3.0 μm , both values being below the mean free path of 9 μm estimated from the mobility. Because the depletion potential extends laterally beyond the gate pattern for high (negative) gate voltages, one can force the constrictions to become progressively narrower (at the same time reducing the electron gas density in the constrictions) — until they are fully pinched off. By this technique it is possible to create point contacts of *variable* width W , something which is not realizable in a metal. Note that W is comparable in magnitude to λ_F (which was 40 nm in the devices studied). These are *quantum point contacts*, as evidenced by their conductance which was discovered to be approximately quantized in units of $2e^2/h$ [10,11].

Electron focusing can be seen as a transmission experiment in electron optics. The classical regime then corresponds to geometrical optics, the quantum regime to wave optics. The optical analogy is useful, both to understand the experiments and to inspire new ones [12]. An alternative point of view is that coherent electron focusing is a prototype of a non-local resistance measurement in the quantum ballistic transport regime, such as studied extensively in narrow-channel geometries [13]. Longitudinal resistances which are negative, not $\pm B$ symmetric, and dependent on the properties of the current and voltage contacts as well as on their separation; periodic and aperiodic magnetoresistance oscillations; absence of local equilibrium — these are all characteristic features of this transport regime which appear in a most extreme and bare form in the electron focusing geometry. One reason for the simplification offered by this geometry is that the current and voltage contacts, being point contacts, are not nearly as invasive as the wide leads in a Hall bar geometry [14]. Another reason is that the electrons interact with only one boundary (instead of two in a narrow channel).

The outline of this paper is as follows. In Sec. 2 the experimental results on electron focusing [5,8] are described as a transmission experiment in a 2DEG. A theoretical description [6,8] is given in Sec. 3, in terms of mode interference in the wave guide formed by the magnetic field at the 2DEG boundary. In Sec. 4 we discuss the quantum Hall effect in the electron focusing geometry [7,8] as a non-local resistance measurement. The theoretical framework used to relate these two alternative descriptions is the Landauer-Büttiker formalism [15,16], which treats a resistance measurement as a transmission experiment. We conclude in Sec. 5.

2 Mirror, lens, and point source

Fig. 2 illustrates electron focusing in two dimensions as it follows from classical mechanics. The arrangement combines three basic elements: mirror, magnetic lens, and point source/detector. The point source (i) injects electrons with the Fermi energy $E_F \equiv mv_F^2/2$ ballistically into the

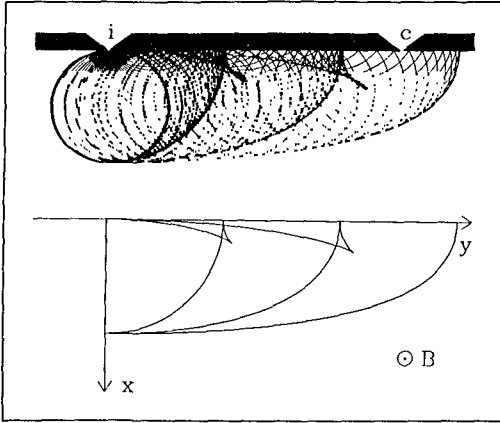


Fig.2

Top: Skipping orbits along the 2DEG boundary. The trajectories are drawn up to the third specular reflection. Bottom: Plot of the caustics, which are the collection of focal points of the trajectories. [From Ref 8.]

2DEG. The injected electrons all have the same Fermi velocity v_F , but in different directions. Electrons are detected if they reach the adjacent collector (c), after one or more specular reflections at the boundary connecting i and c. These *skipping orbits* are composed of translated circular arcs of identical radius $l_{\text{cycl}} \equiv \hbar k_F / eB$, which is the cyclotron radius in a perpendicular magnetic field B ($k_F \equiv mv_F / \hbar$ is the Fermi wave vector). The focusing action of the magnetic field is evident in Fig. 2 (top) from the black lines of high density of trajectories. These lines are known in optics as *caustics*, and are plotted separately in Fig. 2 (bottom). The caustics intersect the 2DEG boundary at multiples of the cyclotron diameter from the injector. As the magnetic field is increased, a series of these focal points shifts past the collector. The electron flux incident on the collector thus reaches a maximum whenever its separation L from the injector is an integer multiple of $2l_{\text{cycl}}$. This occurs when $B = pB_{\text{focus}}$, $p = 1, 2, \dots$, with

$$B_{\text{focus}} = 2\hbar k_F / eL. \quad (1)$$

For a given injected current I_i the voltage V_c on the collector is proportional to the incident flux. The classical picture thus predicts a series of equidistant peaks in the collector voltage as a function of magnetic field.

In Fig. 3 (top) we show such a classical focusing spectrum, calculated for parameters corresponding to the experiment discussed below ($L = 3.0 \mu\text{m}$, $k_F = 0.15 \text{ nm}^{-1}$). The spectrum consists of equidistant focusing peaks of approximately equal magnitude superimposed on the Hall resistance (dashed line). The p -th peak is due to electrons injected perpendicularly to the boundary which have made $p - 1$ specular reflections between injector and collector. Such a classical focusing spectrum is commonly observed in metals [17], albeit with a decreasing

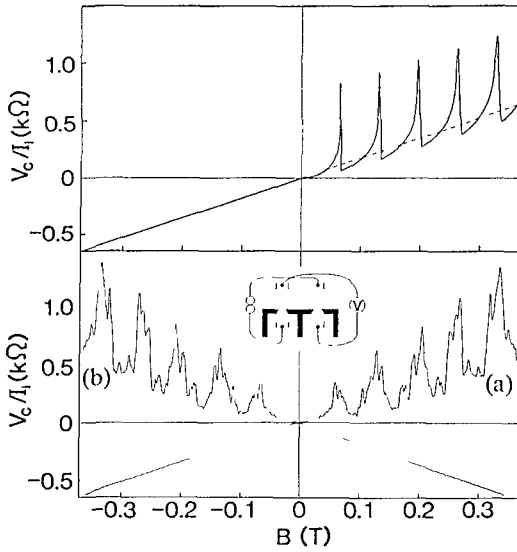


Fig.3

Bottom: Experimental electron focusing spectrum ($T = 50$ mK, $L = 3.0 \mu\text{m}$) in the generalized Hall resistance configuration depicted in the inset. The two traces a and b are measured with interchanged current and voltage leads, and demonstrate the injector-collector reciprocity as well as the reproducibility of the fine structure. Top: Calculated classical focusing spectrum corresponding to the experimental trace a (50 nm wide point contacts were assumed). The dashed line is the extrapolation of the classical Hall resistance seen in reverse fields. [From Ref 8.]

height of subsequent peaks because of partially diffuse scattering at the metal surface. Note that the peaks occur in one field direction only; In reverse fields the focal points are at the wrong side of the injector for detection, and the normal Hall resistance is obtained. The experimental result for a 2DEG is shown in the bottom half of Fig. 3 (trace a ; trace b is discussed below). A series of five focusing peaks is evident at the expected positions. This observation by itself has two important implications:

- A point contact acts as a monochromatic point source of ballistic electrons with a well-defined energy;
- The electrostatically defined 2DEG boundary is a good mirror with little diffuse scattering.

Fig. 3 is obtained in a measuring configuration (inset) in which an imaginary line connecting the voltage probes crosses that between the current source and drain. This is the configuration for a generalized Hall resistance measurement. Alternatively, one can measure a generalized longitudinal resistance, in the configuration shown in the inset of Fig. 4. One then measures the focusing peaks without a superimposed Hall slope. Note that the experimental longitudinal resistance (Fig. 4, bottom) becomes *negative*. This is a classical result of magnetic focusing, as demonstrated by the calculation shown in the top half of Fig. 4. Büttiker [18] has studied negative longitudinal resistances in a different (Hall bar) geometry.

On the experimental focusing peaks a fine structure is evident in Figs. 3 and 4. The fine structure is well reproducible (compare Figs. 3 and

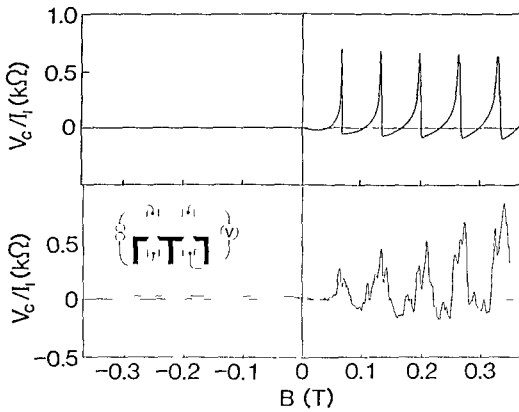


Fig.4
As Fig. 3, but in the longitudinal resistance configuration. [From Ref 8.]

4), but sample dependent. It is only resolved at low temperatures (below 1 K) and small injection voltages (the measurements shown are taken at 50 mK and a few μV AC voltage over the injector). A nice demonstration of the reproducibility of the fine structure is obtained upon interchanging current and voltage leads, so that the injector becomes the collector and vice versa. The resulting focusing spectrum shown in Fig. 3 (trace *b*) is almost the precise mirror image of the original one (trace *a*) — although this particular device had a strong asymmetry in the widths of injector and collector. The symmetry in the focusing spectra is a consequence of the fundamental reciprocity relation derived by Büttiker [16], which generalizes the familiar Onsager-Casimir symmetry relation for the *resistivity tensor* to *resistances* (see Sec. 4).

The fine structure on the focusing peaks in Figs. 3 and 4 is the first indication that electron focusing in a 2DEG is qualitatively different from the corresponding experiment in metals. At higher magnetic fields the resemblance to the classical focusing spectrum is lost, see Fig. 5. A Fourier transform of the spectrum for $B \geq 0.8$ T (inset in Fig. 5) shows that the large-amplitude high-field oscillations have a dominant periodicity of 0.1 T, which is approximately the same as the periodicity B_{focus} of the much smaller focusing peaks at low magnetic fields (B_{focus} in Fig. 5 differs from Fig. 3 because of a smaller $L = 1.5 \mu\text{m}$). This dominant periodicity is the result of quantum interference between the different trajectories in Fig. 2 which take an electron from injector to collector. [In Sec. 3 we show this in a mode picture, which in the WKB approximation is equivalent to calculating the interferences of the (complex) probability amplitude along classical trajectories. The latter ray picture is treated extensively in Ref. 8.] The theoretical analysis implies for the experiment that:

- The injector acts as a *coherent* point source with the coherence maintained over a distance of several microns to the collector.

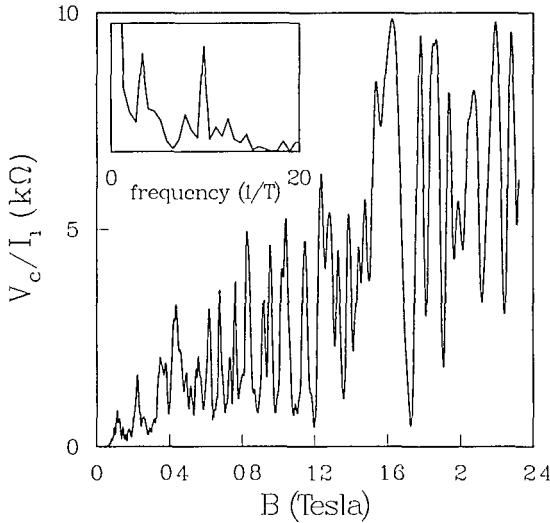


Fig.5

Experimental electron focusing spectrum over a larger field range and for very narrow point contacts (estimated width 20 – 40 nm; $T = 50$ mK, $L = 1.5 \mu\text{m}$). The inset gives the Fourier transform for $B \geq 0.8$ T. The high-field oscillations have the same dominant periodicity as the low-field focusing peaks – but with a much larger amplitude. [From Ref 8.]

3 Edge states and skipping orbits

Magnetic edge states [19,20] are transverse modes of a wave guide of width $\sim l_{\text{cycl}}$ formed by the magnetic field at the 2DEG boundary. The edge states at the Fermi level are labelled by a quantum number $n = 1, 2 \dots N$, with $N = k_F l_{\text{cycl}} / 2$ the total number of propagating modes or edge *channels* (for simplicity we ignore here the discreteness of N). An injector of width below λ_F excites a coherent superposition of these propagating modes (plus evanescent modes, which using the ray treatment of Ref. 8 are found to give only a small contribution for the large $k_F L$ considered, and will be neglected here). The wave function Ψ is of the form

$$\Psi(x, y) = \sum_{n=1}^N a_n f_n(x) e^{ik_n y}. \quad (2)$$

Here k_n is the wave number for propagation of mode n in the y -direction (along the 2DEG boundary, see Fig. 2 for our choice of axes), $f_n(x)$ is the transverse amplitude profile of mode n , and a_n its excitation factor. For $k_F L \gg 1$ the phase factors $\exp(ik_n L)$ vary rapidly as a function of n . Constructive interference of modes at the collector then requires that $k_n L$ differs by multiples of 2π for a series of n . To find out what this condition implies for the magnetic field, we determine k_n in WKB approximation (which should be sufficiently accurate for this purpose).

Consider again the classical skipping orbits (Fig. 2). The position (x, y) of the electron on the circle with center coordinates (X, Y) can be expressed in terms of its velocity \mathbf{v} by

$$x = X + v_y / \omega_c, \quad y = Y - v_x / \omega_c, \quad (3)$$

with $\omega_c = eB/m$ the cyclotron frequency. Note that the separation X of the center from the boundary is constant on a skipping orbit, only the center coordinate Y parallel to the boundary changes at each specular reflection. The canonical momentum of the electron is $\mathbf{p} = m\mathbf{v} - e\mathbf{A}$. In the Landau gauge $\mathbf{A} = (0, Bx, 0)$ we have

$$p_x = mv_x, \quad p_y = -eB X. \quad (4)$$

The wave number k corresponds classically to the canonical momentum component $p_y = \hbar k$, so that in view of Eq. (4) we have the correspondence $k = -(eB/\hbar) X$. Since the motion projected on the x -axis is periodic, one can apply the Bohr-Sommerfeld quantization rule [21]

$$\frac{1}{h} \oint p_x dx + \gamma = 2\pi n. \quad (5)$$

The integral is over one period of the motion, n is an integer, and γ is the sum of the phase shifts acquired at the two turning points of the motion. The phase shift upon reflection at the boundary is π (for an infinite barrier potential, to ensure that incident and reflected waves cancel); The other turning point is a caustic of the skipping orbits with constant X , leading to a phase shift of $-\pi/2$ [22]. This totals to $\gamma = \pi/2$. Using also Eqs. (3) and (4) we may thus write Eq. (5) in the form

$$\frac{eB}{h} \oint (Y - y) dx = 2\pi \left(n - \frac{1}{4} \right), \quad n = 1, 2, \dots N. \quad (6)$$

This quantization rule has the simple geometrical interpretation [20] that the flux enclosed by one arc of the skipping orbit and the boundary equals $(n - 1/4)$ times the flux quantum h/e (see insets in Fig. 6).

Eq. (6) determines, for a given magnetic field, the energy $E = mv^2/2$ as a function of the quantum number n and the wave number $k = -(eB/\hbar) X$. To carry out the integration in Eq. (6) we express y in terms of x by means of Eq. (3). The resulting energy spectrum $E_n(k)$ is given by

$$\frac{2E}{\hbar\omega_c} \left(\arccos \xi - \xi (1 - \xi^2)^{1/2} \right) = 2\pi \left(n - \frac{1}{4} \right), \quad \xi \equiv \hbar k (2mE)^{-1/2}, \quad (7)$$

and is plotted in Fig. 6 (solid curves). Also plotted in Fig. 6 is the exact solution of the Schrödinger equation (dashed curves, taken from Ref.

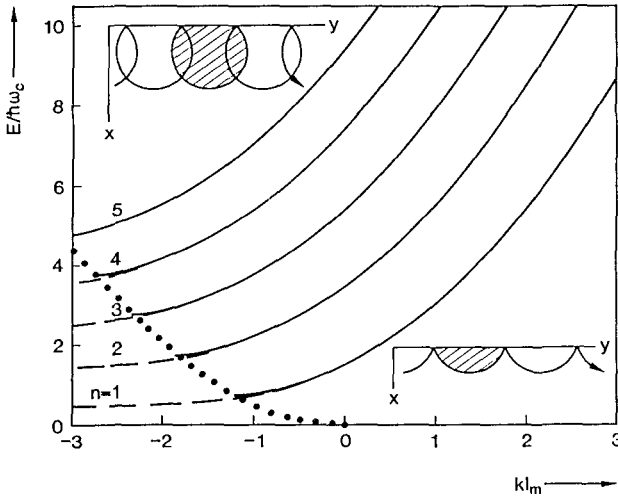


Fig.6 Energy spectrum $E_n(k)$ of magnetic edge states at an infinite barrier potential boundary. Note that $kl_m = -X/l_m$, with X the separation of the orbital center from the boundary and $l_m \equiv (\hbar/eB)^{1/2}$ the magnetic length. The insets show classical skipping orbits for positive and negative k . In the semi-classical approximation the magnetic flux through the shaded areas is quantized. The result from Eq. (7) (solid curves) is indistinguishable from the exact solution (dashed curves, from Ref. 23), unless k is within $1/l_m$ of the transition from skipping to cyclotron orbits (dotted curve). [From Ref. 8.]

23). The (semi-classical) WKB approximation (7) is indistinguishable on this scale from the exact solution, except just before the transition from skipping orbits to bulk cyclotron orbits at $X = mv/eB$ (dotted curve in Fig. 6). The quantized wave numbers k_n at the Fermi energy satisfy $E_n(k_n) = E_F$, so that k_n is determined by Eq. (7) with the substitutions $E \equiv E_F$, $\xi \equiv k_n/k_F$. As shown in Fig. 7 the resulting dependence on n of the phase $k_n L$ is close to linear in a broad interval,

$$k_n L = \text{constant} - 2\pi n B/B_{\text{focuss}} + k_F L \times \text{order}(1 - 2n/N)^3. \quad (8)$$

It follows from this expansion that if B/B_{focuss} is an integer, a fraction of order $(1/k_F L)^{1/3}$ of the N edge channels interfere constructively at the collector. Because of the $1/3$ power, this is a substantial fraction even for the large $k_F L \sim 10^2$ of the experiment. The relevant states have quantum number n in an interval centered around $N/2$, corresponding classically to skipping orbits which reach the boundary at approximately right angles. The edge states outside the domain of linear n -dependence of the phase give rise to fine structure without a simple periodicity.

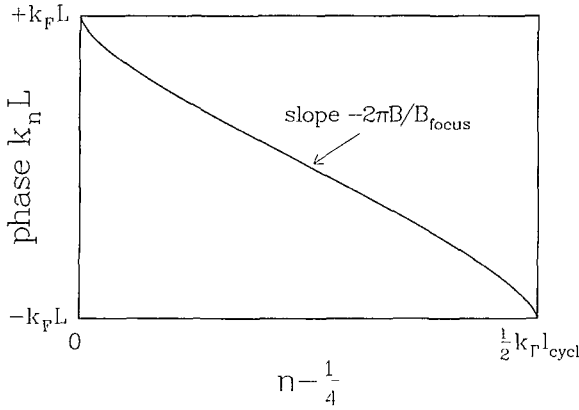


Fig.7
Phase $k_n L$ of the edge channels at the collector, calculated from Eq. (7). Note the domain of approximately linear n -dependence of the phase, responsible for the oscillations with B_{focus} -periodicity. [From Ref 8.]

To determine the amplitude of the oscillations in the collector voltage, we need to know the excitation factors of the modes by the injector and the transmission amplitude through the collector. In Ref. 8 we calculated these quantities using a point-dipole injector and a transmission amplitude proportional to the derivative $\partial\Psi/\partial x$ of the unperturbed wave function at the collector – thereby neglecting the finite width of the injector and collector point contacts. The result obtained there can be written in the form

$$\frac{V_c}{I_i} = \frac{h}{2e^2} \left| \frac{1}{N} \sum_{n=1}^N e^{ik_n L} \right|^2. \quad (9)$$

In Fig. 8 we have plotted the focusing spectrum from Eq. (9), corresponding to the experimental Fig. 5. The inset shows the Fourier transform for $B \geq 0.8$ T. There is no detailed one-to-one correspondence between the experimental and theoretical spectra. No such correspondence was to be expected in view of the sensitivity of the experimental spectrum to small variations in gate voltage (which defines the point contacts and the 2DEG boundary). Those features of the experimental spectrum which are insensitive to the precise measurement conditions are, however, well reproduced by the calculation: We recognize in Fig. 8 the low-field focusing peaks and the large-amplitude high-field oscillations with the same periodicity. [The reason that the periodicity B_{focus} in Fig. 8 is somewhat larger than in Fig. 5 is most likely the experimental uncertainty in the effective point contact separation of the order of the split-gate opening (250 nm).] The high-field oscillations range from about 0 to 10k Ω in both theory and experiment.

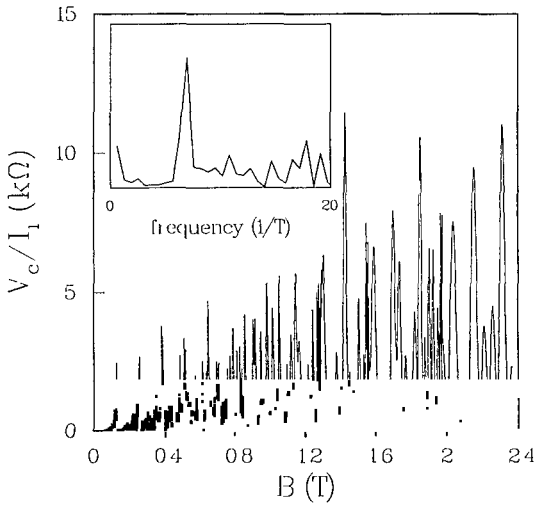


Fig.8 Focusing spectrum calculated from Eq. (9), for parameters corresponding to the experimental Fig. 5. The inset shows the Fourier transform for $B \geq 0.8$ T. Infinitesimally small point contact widths are assumed in the calculation.

This maximum amplitude is not far below the theoretical upper bound of $h/2e^2 \approx 13$ k Ω , which follows from Eq. (9) if we assume that *all* the modes interfere constructively. This indicates that a *maximal phase coherence* is realized in the experiment, and implies that:

- The experimental injector and collector point contacts resemble the idealized point source/detector in the calculation;
- Scattering events other than specular scattering on the boundary can be largely ignored (since any other inelastic *as well as elastic* scattering events would scramble the phases and reduce the oscillations with B_{focus} – periodicity).

It follows from Eq. (9) that if interference of the modes is ignored, the normal quantum Hall resistance $h/2Ne^2$ is obtained. This is *not* a general result, but depends specifically on the properties of the injector and collector point contacts – as we will discuss in the following section.

4 Quantum point contacts as Landau level selectors

Mode interference becomes unimportant if the magnetic field is sufficiently strong, and the point contacts are sufficiently wide, that the electrostatic potential in the point contact region does not cause scattering between the modes. The requirement for such *adiabatic* transport is that the potential varies slowly on the scale of l_{cycl} (in the quantum Hall effect regime where $N \sim 1$ and $E_{\text{F}} \sim \hbar\omega_c$, the cyclotron radius is the magnetic length $l_m \equiv (\hbar/eB)^{1/2}$). In this field regime the form of the

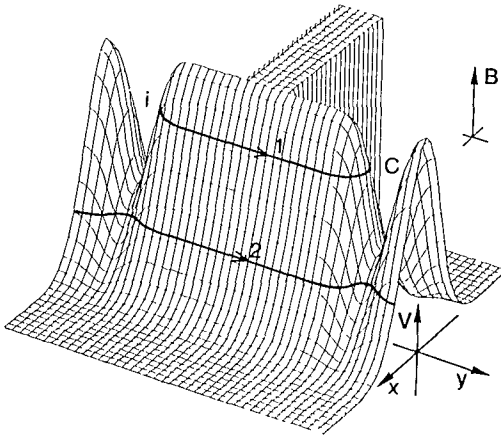


Fig.9 Schematic potential landscape, showing the 2DEG boundary and the saddle-shaped injector and collector point contacts. In a strong magnetic field the edge channels are extended along equipotentials (Eq. (10)), as indicated here for $n = 1, 2$ (the arrows point in the direction of motion). In this case a Hall conductance of $(2e^2/h)N$ with $N=1$ would be measured by the point contacts – in spite of the presence of 2 occupied Landau levels in the bulk 2DEG.

electrostatic potential $V(x, y)$ defining the point contacts becomes important, and the point injector/detector model used in the previous section – while adequate at lower magnetic fields – is insufficient.

Schematically, $V(x, y)$ is represented in Fig. 9. Fringing fields from the split-gate create a potential barrier in the point contacts, so that V has a saddle form as shown. The heights of the barriers E_i , E_c in the injector and collector are separately adjustable by means of the voltages on the split-gates, and can be determined from the conductances of the individual point contacts [24]. The width of the point contacts does not play a role, because it is larger than l_{cycl} . The adiabatic transport is along equipotentials as indicated in Fig. 9 (arrows point in the direction of motion, determined by the potential gradient). The energy of the equipotential is the *guiding center energy* E_G , which is given for edge channel n by

$$E_G = E_F - (n - \frac{1}{2}) \hbar \omega_c \quad (10)$$

(Zeeman spin-splitting of the energy levels should be included at large magnetic fields, but is ignored here for simplicity). The edge channels can only be transmitted through a point contact if E_G exceeds the potential barrier height (disregarding tunneling through the barrier). The injector thus injects $N_i \approx (E_F - E_i) / \hbar \omega_c$ edge channels into the 2DEG, while the collector is capable of detecting $N_c \approx (E_F - E_c) / \hbar \omega_c$ channels. Along the boundary of the 2DEG, however, a larger number of $N \approx E_F / \hbar \omega_c$ edge channels, equal to the number of bulk Landau levels in the 2DEG, are available for the current transport. The selective population, and detection, of Landau levels leads to deviations from the normal Hall resistance.

These considerations can be put on a theoretical basis by applying the general Landauer-Büttiker formalism [15,16], which relates resistances

to transmission probabilities into current and voltage probes. Consider the geometry in Fig. 1 of a three-terminal conductor with point contacts in two of the probes. The probes are connected by perfect leads to reservoirs which have a constant electro-chemical potential. We denote by μ_i and μ_c the chemical potentials of the two reservoirs connected, respectively, to the injector and collector point contact, and by μ_d the chemical potential of the third reservoir (the current drain). Following Büttiker [16], we can relate the currents I_α ($\alpha = i, c, d$) in the three leads to these chemical potentials via the transmission probabilities $T_{\alpha \rightarrow \beta}$ (from reservoir α to reservoir β) and reflection probabilities R_α (from reservoir α back to the same reservoir),

$$\frac{h}{2e} I_\alpha = (N_\alpha - R_\alpha) \mu_\alpha - \sum_{\beta \neq \alpha} T_{\beta \rightarrow \alpha} \mu_\beta, \quad (11)$$

N_α being the number of occupied modes in the lead α . We now impose the condition that the collector draws no net current, which implies $I_c = 0$ and $I_d = -I_i$, and choose our zero of energy such that $\mu_d = 0$. One then finds from Eq. (11) the two equations

$$\mu_c = \frac{T_{i \rightarrow c}}{N_c - R_c} \mu_i, \quad \frac{h}{2e} I_i = (N_i - R_i) \mu_i - T_{c \rightarrow i} \mu_c, \quad (12)$$

and obtains for the ratio of collector voltage $V_c = \mu_c / e$ (measured relative to the voltage of the current drain) to injected current I_i the result

$$\frac{V_c}{I_i} = \frac{2e^2}{h} \frac{T_{i \rightarrow c}}{G_i G_c - \delta}. \quad (13)$$

Here $\delta \equiv (2e^2/h)^2 T_{i \rightarrow c} T_{c \rightarrow i}$, and $G_i \equiv (2e^2/h)(N_i - R_i)$ and $G_c \equiv (2e^2/h)(N_c - R_c)$ denote the conductances of the injector and collector point contact, respectively. The injector-collector reciprocity in electron focusing, demonstrated in Fig. 3, is manifest in Eq. (13), since G_i and G_c are even in B and [16] $T_{i \rightarrow c}(B) = T_{c \rightarrow i}(-B)$.

In the electron focusing geometry the term δ in Eq. (13) can be neglected, since $T_{c \rightarrow i} \approx 0$. An additional simplification is possible in the adiabatic transport regime. We consider the case that the barrier in one of the two point contacts is sufficiently higher than in the other, to ensure that electrons which are transmitted over the highest barrier will have a negligible probability of being reflected at the lowest barrier. Then $T_{i \rightarrow c}$ is dominated by the transmission probability over the highest barrier, $T_{i \rightarrow c} \approx \min(N_i - R_i, N_c - R_c)$. Substitution into Eq. (11) gives the remarkable result that the *Hall conductance* $G_{\text{H}} \equiv I_i / V_c$ measured in the electron focusing geometry can be expressed entirely in terms of the *contact conductances* G_i and G_c ,

$$G_{\text{H}} \approx \max(G_i, G_c). \quad (14)$$

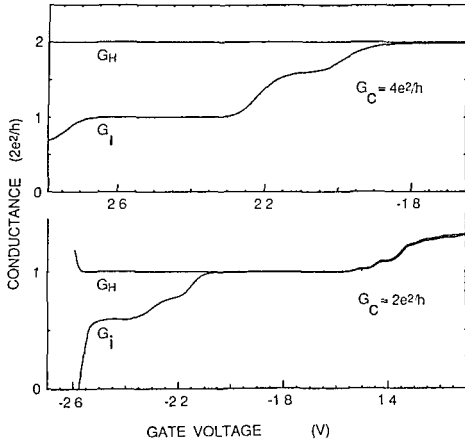


Fig.10.

Experimental correlation between the conductances G_i , G_c of injector and collector, and the Hall conductance $G_H \equiv I_x/V_c$, shown to demonstrate the validity of Eq. (14) ($T = 1.3$ K, $L = 1.5$ μm). The magnetic field was kept fixed (top: $B = 2.5$ T, bottom: $B = 3.8$ T). By increasing the gate voltage on one half of the split-gate defining the injector, G_i was varied at constant G_c . [From Ref 7.]

Eq. (14) tells us that quantized values of G_H occur not at $(2e^2/h)N$, as one would expect from the N Landau levels in the 2DEG — but at the smaller value of $(2e^2/h) \max(N_i, N_c)$. Moreover, there is no quantized Hall conductance unless the largest of the two contact conductances is quantized. As shown in Fig. 10, this is indeed observed experimentally. Notice in particular how any deviation from quantization in $\max(G_i, G_c)$ is faithfully reproduced in G_H . The implication of this experiment is that:

- Point contacts can be used to *selectively* populate and detect Landau levels at the 2DEG boundary;
- Adiabatic transport (i.e. transport in the absence of inter-Landau level scattering) has been realized over a distance of 1.5 μm along the 2DEG boundary.

As discussed by Büttiker [25], the fundamental origin for deviations from the normal quantum Hall effect is the absence of local equilibrium among the edge channels. Selective population is indeed an extreme example of a non-equilibrium population. Recent related experiments [26,27] have demonstrated that a non-equilibrium population of edge channels can be maintained on even longer length scales, possibly as large as several hundred microns. It remains a theoretical challenge to explain these surprisingly long relaxation lengths.

5 Conclusion

In Sec. 1 we emphasized that the *length scales* relevant for the electron focusing experiment are very different in a metal and in a 2DEG. Both the ratios λ_T/L and λ_T/W are much larger in a 2DEG, typically by factors of 10^4 and 10^2 , respectively. As we showed in Secs. 2 and 3, coherent electron focusing is possible in a 2DEG because of this rela-

tively large value of the Fermi wave length. The adiabatic transport discussed in Sec. 4 is also made possible by the large λ_F , since now $l_{\text{cycl}} = h/eB\lambda_F$ can become comparable to W at magnetic fields of a few Tesla. To achieve the same in a metal would require fields over 100 T. The difference in *energy scale* between a metal and a 2DEG manifests itself in the dependence of the focusing spectrum on the voltage drop over the injector. In metals, electrons are injected at energies above E_F which are generally much less than $E_F \sim 5 \text{ eV}$ [28]. In contrast, $E_F \sim 10 \text{ meV}$ in a 2DEG, and DC-biasing the small AC injection voltage used in the electron focusing experiment should lead to a noticeable shift in the focusing peaks, in analogy with a β -spectrometer. In the simplest model one would have (cf. Eq. (1)) $B_{\text{focus}} \propto (E_F + eV_{\text{DC}})^{1/2}$, so that for a DC bias $V_{\text{DC}} = 1 \text{ mV}$ one would expect a 5% shift in the focusing periodicity — provided the hot electrons remain ballistic. This is indeed observed [29], although deviations from this simple behavior are found for larger DC biases (possibly related to the non-linear current-voltage characteristics of the point contacts themselves[30]). The observation of hot-electron transport over several microns is remarkable, and unexpected from related work in different systems [31].

The main result of the theoretical analysis of coherent electron focusing in Sec. 3 is the demonstration of high-field oscillations with B_{focus} -periodicity, but much larger amplitude than the low-field focusing peaks. This is also the feature of the experimental focusing spectra which is insensitive to small changes in gate voltage and which is found in both the devices studied. The theory can be improved in several ways. This will affect the detailed form of the spectra, but probably not the fundamental periodicity. Since the exact wave functions of the edge states are known (Weber functions), one could go beyond the WKB approximation. This will become important at large magnetic fields, when the relevant edge states have small quantum numbers. In this regime one would also have to take into account a possible B -dependence of E_F relative to the conduction band bottom (due to pinning of the Fermi energy at the Landau levels). It would be interesting to find out to what extent this bulk effect is reduced at the 2DEG boundary by the presence of edge states to fill the gap between the Landau levels.

Another direction of improvement is towards a more realistic modelling of the injector and collector point contacts. Since the maximum amplitude of the theoretical and experimental oscillations is about the same (compare Figs. 5 and 8), the loss of spatial coherence due to the finite point contact size does not seem to be particularly important in this experiment (infinitesimal point contact width was assumed in the calculation). On the other hand, the experimental focusing spectrum does not contain as much rapid oscillations as the calculation would predict.

Energy averaging due to a finite temperature is not the reason for this difference (temperatures on the order of 10 K are necessary to smear out the rapid oscillations). We surmise that the rapid oscillations are reduced by the *collimation* effect proposed originally [32] to explain the non-additivity of the resistance of two opposite point contacts in series [33] (and more recently invoked [34] to explain the quenching of the Hall resistance in a narrow-channel geometry [13]). Both the flaring of a point contact to form a horn, and the presence of a potential barrier in the point contact region tend to collimate the injected electron beam [32], so that electrons are predominantly injected at right angles to the boundary. The quantum mechanical correspondence discussed in Sec. 3 then implies that such a point contact excites (and detects) predominantly the edge channels with quantum number n close to $N/2$, at the expense of channels with smaller or larger n . Since the former edge channels are responsible for the oscillations with B_{focus} -periodicity, while the latter give rise to rapid aperiodic oscillations (see Fig. 7 and the accompanying discussion), the collimation effect provides one mechanism for the absence of rapid oscillations in the experimental focusing spectrum.

Acknowledgement

The authors have greatly benefitted from their collaboration with M.E.I. Broekart, C.T. Foxon, C.J.P.M. Harmans, J.J. Harris, L.P. Kouwenhoven, P.H.M. van Loosdrecht, D. van der Marel, J.E. Mooij, M.F.H. Schuurmans, J.A. Pals, E.M.M. Willems, and J.G. Williamson.

References

- [1] Yu.V. Sharvin, Zh.Eksp.Teor.Fiz. **48**, 984 (1965) [Sov.Phys.JETP **21**, 655 (1965)]
- [2] V.S. Tsoi, Pis'ma Zh.Exp.Teor.Fiz. **19**, 114 (1974) [JETP Lett. **19**, 70 (1974)]
- [3] P.C. van Son, H. van Kempen, and P. Wyder, Phys.Rev.Lett. **58**, 1567 (1987)
- [4] Physics and Technology of Submicron Structures, ed. by H. Heinrich, G. Bauer, and F. Kuchar (Springer, Berlin 1988); Nanostructure Physics and Fabrication, ed. by M. Reed and W.P. Kirk (Academic Press, New York, to be published)
- [5] H. van Houten, B.J. van Wees, J.E. Mooij, C.W.J. Beenakker, J.G. Williamson, and C.T. Foxon, Europhys.Lett. **5**, 721 (1988)
- [6] C.W.J. Beenakker, H. van Houten, and B.J. van Wees, Europhys.Lett. **7**, 359 (1988)
- [7] B.J. van Wees, E.M.M. Willems, C.J.P.M. Harmans, C.W.J. Beenakker, H. van Houten, J.G. Williamson, C.T. Foxon, and J.J. Harris, Phys.Rev.Lett. **62** 1181 (1989)

- [8] *H. van Houten, C.W.J. Beenakker, J.G. Williamson, M.E.I. Broekaart, P.H.M. van Loosdrecht, B.J. van Wees, J.E. Mooij, C.T. Foxon, and J.J. Harris*, Phys.Rev. **B** (April 15, 1989)
- [9] *T.J. Thornton, M. Pepper, H. Ahmed, D. Andrews, and G.J. Davies*, Phys.Rev.Lett. **56**, 1198 (1986); *H.Z. Zheng, H.P. Wei, D.C. Tsui, and G. Weimann*, Phys.Rev. **B34**, 5635 (1986)
- [10] *B.J. van Wees, H. van Houten, C.W.J. Beenakker, J.G. Williamson, L.P. Kouwenhoven, D. van der Marel, and C.T. Foxon*, Phys.Rev.Lett. **60**, 848 (1988)
- [11] *D.A. Wharam, T.J. Thornton, R. Newbury, M. Pepper, H. Ahmed, J.E.F. Frost, D.G. Hasko, D.C. Peacock, D.A. Ritchie, and G.A.C. Jones*, J.Phys. **C21**, L209 (1988)
- [12] *H van Houten and C.W.J. Beenakker*, in: Analogies in Optics and Microelectronics, ed. by *W. van Haeringen and D. Lenstra* (Kluwer, Deventer, to be published)
- [13] *G. Timp, A.M. Chang, P. Mankiewich, R. Behringer, J.E. Cunningham, T.Y. Chang, and R.E. Howard*, Phys.Rev.Lett. **59**, 732 (1987); *M.L. Roukes, A. Scherer, S.J. Allen, Jr., H.G. Craighead, R.M. Ruthen, E.D. Beebe, and J.P. Harbison*, Phys.Rev.Lett. **59**, 3011 (1987); *C.J.B. Ford, T.J. Thornton, R. Newbury, M. Pepper, H. Ahmed, D.C. Peacock, D.A. Ritchie, J.E.F. Frost, and G.A.C. Jones*, Phys.Rev. **B38**, 8518 (1988); *G. Timp*, in: Mesoscopic Phenomena in Solids, ed. by *P.A. Lee, R.A. Webb, and B.L. Al'tshuler* (Elsevier, New York, to be published)
- [14] *G. Timp, H.U. Baranger, P. deVegvar, J.E. Cunningham, R.E. Howard, R. Behringer, and P.M. Mankiewich*, Phys.Rev.Lett. **60**, 2081 (1988); *Y. Takagaki, K. Gamo, S. Namba, S. Ishida, S. Takaoka, K. Murase, K. Ishibashi, and Y. Aoyagi*, Solid State Comm. **68**, 1051 (1988)
- [15] *R. Landauer*, IBM J.Res.Dev. **1**, 223 (1957); **32**, 306 (1988); Z.Phys. **B68**, 217 (1987)
- [16] *M. Büttiker*, Phys.Rev.Lett. **57**, 1761 (1986); IBM J.Res.Dev. **32**, 317 (1988); See also: *A.D. Stone and A. Szafer*, IBM J.Res.Dev. **32**, 384 (1988)
- [17] *P.A.M. Benistant, G.F.A. van de Walle, H. van Kempen, and P. Wyder*, Phys.Rev. **B33**, 690 (1986)
- [18] *M. Büttiker*, Phys.Rev. **B38**, 12724 (1988)
- [19] *R.E. Prange and T.-W. Nee*, Phys.Rev. **168**, 779 (1968)
- [20] *M.S. Khaikin*, Adv.Phys. **18**, 1 (1969)
- [21] *A.M. Kosevich and I.M. Lifshitz*, Zh.Eksp.Teor.Fiz. **29**, 743 (1955) [Sov.Phys.JETP **2**, 646 (1956)]
- [22] *L.D. Landau and E.M. Lifshitz*, The Classical Theory of Fields (Pergamon, Oxford 1987) § 54
- [23] *A.H. MacDonald and P. Streda*, Phys.Rev. **B29**, 1616 (1984)
- [24] *B.J. van Wees, L.P. Kouwenhoven, H. van Houten, C.W.J. Beenakker, J.E. Mooij, C.T. Foxon, and J.J. Harris*, Phys.Rev. **B38**, 3625 (1988)
- [25] *M. Büttiker*, Phys.Rev. **B38**, 9375 (1988)
- [26] *S. Komiyama, H. Hirai, S. Sasa, and S. Hiyamizu* (preprint)
- [27] *B.J. van Wees, E.M.M. Willems, L.P. Kouwenhoven, C.J.P.M. Harmans, J.G. Williamson, C.T. Foxon, and J.J. Harris* Phys.Rev. **B** (April 15, 1989)
- [28] *P.C. van Son, H. van Kempen, and P. Wyder*, J.Phys. **F17**, 1471 (1987)
- [29] *J.G. Williamson et al.* (unpublished)
- [30] *L.P. Kouwenhoven, B.J. van Wees, C.J.P.M. Harmans, J.G. Williamson, H. van Houten, C.W.J. Beenakker, C.T. Foxon, and J.J. Harris*, Phys.Rev. **B** (April 15, 1989)

- [31] *A. Palevski, M. Heiblum, C.P. Umbach, C.M. Knoedler, A.N. Broers, and R.H. Koch* (preprint)
- [32] *C.W.J. Beenakker and H. van Houten*, Phys.Rev. **B** (to be published)
- [33] *D.A. Wharam, M. Pepper, H. Ahmed, J.E.F. Frost, D.G. Hasko, D.C. Peacock, D.A. Ritchie, and G.A.C. Jones*, J.Phys. **C21**, L887 (1988)
- [34] *H.U. Baranger and A.D. Stone* (preprint); *A.M. Chang and T.Y. Chang* (preprint); *C.J.B. Ford, S. Washburn, M. Büttiker, C.M. Knoedler, and J.M. Hong* (preprint)

FESTKÖRPERPROBLEME 29

ADVANCES IN SOLID STATE PHYSICS

Editors:

Prof. Dr. W. Shockley, Boulder (Vol. I - Vol. VI)

Prof. Dr. G. H. Geiger, München (Vol. VII - Vol. XIII)

Prof. Dr. H. J. Goldsmid, Cambridge (Vol. XIV - Vol. XXV)

Prof. Dr. W. Shockley, Boulder (Vol. XXVI - Vol. XXX)

Prof. Dr. P. Grosse, Aachen (Vol. XXXI - Vol. XXX)

Prof. Dr. H. Koster, Regensburg (Vol. XXXI - Vol. XXX)

Festkörperphysik: 29

München, 1992, VIII, 345 S., 15,2 x 24,9 cm, Hartcover, DM 11,95

Festkörperphysik: 28

München, 1991, VIII, 345 S., 15,2 x 24,9 cm, Hartcover, DM 11,95

Festkörperphysik: 27

München, 1990, VIII, 345 S., 15,2 x 24,9 cm, Hartcover, DM 11,95

Festkörperphysik: 26

München, 1989, VIII, 345 S., 15,2 x 24,9 cm, Hartcover, DM 11,95

Festkörperphysik: 25

München, 1988, VIII, 345 S., 15,2 x 24,9 cm, Hartcover, DM 11,95

Festkörperphysik: 24

München, 1987, VIII, 345 S., 15,2 x 24,9 cm, Hartcover, DM 11,95

Festkörperphysik: 23

München, 1986, VIII, 345 S., 15,2 x 24,9 cm, Hartcover, DM 11,95

Festkörperphysik: 22

München, 1985, VIII, 345 S., 15,2 x 24,9 cm, Hartcover, DM 11,95

Please send to:



**Friedr. Vieweg & Sohn
Verlagsgesellschaft mbH
P.O.B. 5829**

**D-6200 Wiesbaden
Federal Republic of Germany**

» vieweg

Please type
or print in
capital
letters
your
name and
address



Please send immediately

No. of copies	Title	Price
	Festkörperprobleme 29 Advances in Solid State Physics	DM 168,—
	Festkörperprobleme 28	DM 98,—
	Festkörperprobleme 27	DM 178,—
	Festkörperprobleme 26	DM 178,—
	Festkörperprobleme XXII	DM 124,—
	Festkörperprobleme XXI	DM 148,—
	Festkörperprobleme XX	DM 128,—

Date

Signature